# Spatio-temporal activity arithmetics with dopamine and acetylcholine

## Introduction

Meaningful behavior is most often comprised of a sequence of actions (Lashley 1951). In fact, the temporally ordered activation of ensembles of neurons, called activity sequences, have been observed in several brain regions performing a variety of tasks (review: Bhalla 2019). Besides typical examples of sequences in sensory systems (e.g. auditory system: Bouchard and Brainard 2016), there are further findings on activity sequences in memory recall (Pastalkova et al. 2008), and in learning (Modi, Dhawale, and Bhalla 2014), to name but a few.

A feedforward network (Kumar, Rotter, and Aertsen 2010) is a simple model that is able to generate such sequences (Diesmann, Gewaltig, and Aertsen 1999). Given the connectivity in the brain, a recurrent network model is biologically more plausible. There are several approaches to tune recurrent networks to have temporal activity sequences emerge. Often, this implies a kind of adaption, e.g. short-term synaptic depression (York and van Rossum 2009), to create temporal activity patterns. But also learning rules, for example synaptic timing-dependent plasticity rules work to steer the network to more diverse sequential activity (Haga and Fukai 2018).

Recently, Spreizer and colleagues demonstrated a connectivity rule for networks of spiking neurons which lead to a reliable generation of activity sequences (Spreizer, Aertsen, and Kumar 2019). A neuronal network built up on Spreizer et al.'s (2019) rule is however hardwired, and thus not flexible. In this study, we introduce an additional layer to the network to accomplish a network that hasa fixed structure on the one hand , and on the other hand it features dynamic changes in the activity sequences.

In the brain, neuromodulators tackle this task. It is well known, that the neuromodulator dopamine (DP) has a crucial role in motivation, normal motor function, and reward-related learning. In the context of movement control, among other aspects, DP influences the excitability (Day et al. 2008) and the strength of cortico-striatal inputs (Redgrave et al. 2010). In the striatum, the antagonistic balance of DP and acetylcholine (ACh) is important for normal striatal function (Centonze et al. 2003). Since these neuromodulators have opposing effects on the excitability (Zhou, Wilson, and Dani 2003; Reynolds, Hyland, and Wickens 2001), we have a biological example for the additional layer in our network to have either increasing or decreasing excitability.

However, the way in which dopamine is released is under debate. The study of Patriarchi et al. (2018) argues in favor of a textured release, whereas Hamid and colleagues (Hamid, Frank, and Moore 2021)

found DP being released in a wave-like pattern. In this study, we follow the textured release of DP, and assume a similar pattern for ACh.

Neural manifolds embody activity patterns of correlated activity, and are present in various cortices and tasks, such as movements and learning (Gallego et al. 2017). The introduction of an additional layer may lead to changes in the activity of the neurons. In the context of movements, such perturbations may be accompanied with a change of the neural manifold. Hence, we are interested in the question to which degree the introduction of an neuromodulatory patch can alter a neural manifold.

## Material&Methods

For the simulations, we designed a network, that allows and supports the spontaneous emergence of spatio-temporal activity sequences (STAS). Spreizer and colleagues investigated neuronal networks of 'leaky-integrate-and-fire' neurons (Spreizer, Aertsen, and Kumar 2019). They set up local recurrent random networks (LCRN) with feedforward networks embedded in them. Moreover, they used a connectivity rule, which promotes the emergence of STAS. It introduces inhomogeneities in the spatial distribution of axons. As they pointed out, two conditions are necessary to ensure the emergence of STAS in a network of excitatory and inhibitory neurons (EI-network) with spiking neurons: (1) each excitatory neuron projects a small fraction of its axons in a preferred direction ϕ, and (2) ϕs for neurons in the vicinity are similar, whereas ϕs are unrelated for neurons far from each other.

To consolidate the principles and arguments, under which circumstance STAS occur, we exploit a different computational model, introduced by Amari (1972), and Wilson and Cowan (1973), often referred to as 'rate model'. The dynamics can be generally described by the differential equation

$$\tau_r \cdot \frac{dR(t)}{dt} = -R(t) + F[W \bullet R(t) + I_{ext}(t)] \qquad \text{(Eq. 1)}$$

with $\tau_r$ being a time constant, resembling the reaction time of the network, *R(t)* being the current membrane potential, or rate, of the neuronal population, *F* being a gain function, W being the connectivity matrix of the network, and $I_{ext}$ being the external input. As Wilson and Cowan (1972) pointed out in an earlier study, the gain function *F* is sigmoidal in shape

$$F(x) = \frac{1}{1 + e^{-s \cdot (x - x_0)}} \qquad \text{(Eq. 2)}$$

with *s* being the steepness, and $x_0$ the offset of the sigmoid. The connectivity matrix comprises all excitatory and inhibitory synaptic connections, also accounting for the synaptic weights. *W•r(t)* is the scalar product of the synapses and the current rate. The result of eq. 1 is the change of the current rate. The output, or rates, is bounded between 0 and 1 (Wilson and Cowan 1973), and thus lives in a continuous space, whereas spiking neuronal models generate discrete events as output, namely action potentials. Yet, the dynamics of the network were defined, thus, the next step is to derive the parameter

of the network to consolidate the findings of Spreizer and colleagues (Spreizer, Aertsen, and Kumar 2019).

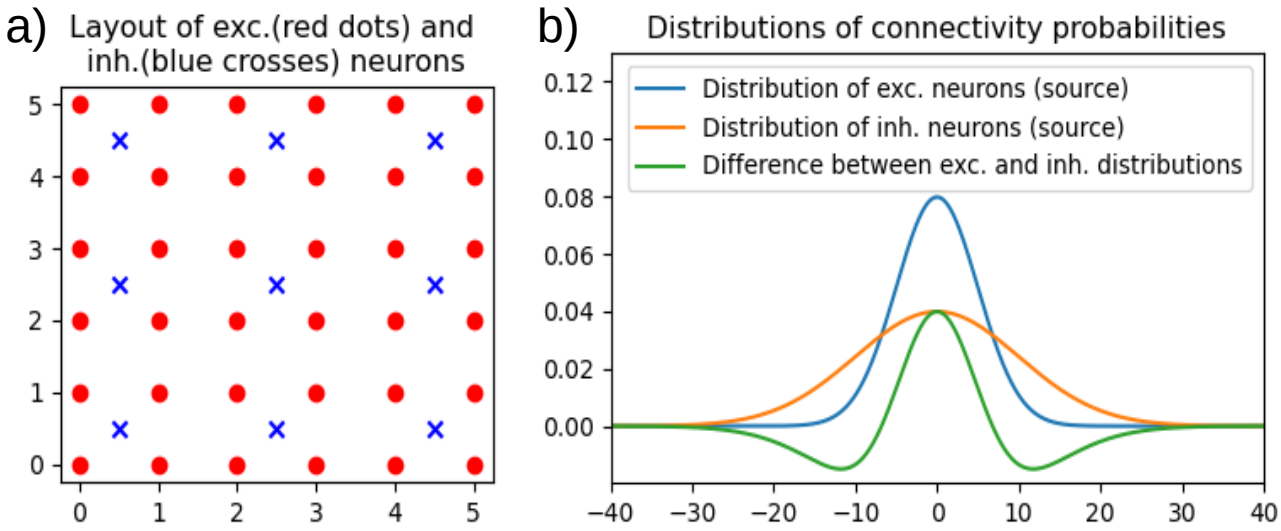


*Figure 1: a) Layout of excitatory and inhibitory neurons. b) Distance-dependent connectivity probabilities of a Gaussian distribution (scaled to the grid of excitatory neurons)*

In order to generate a LCRN with a wide range of opportunities, we aimed for a network with a medium number of sequences emerging. These sequences should have a medium velocity and tend to change their direction. In the following, we specify the set of parameters to attain a network that elicit the desired properties. The study of Spreizer et al. (2019) provides an analysis of many characteristics resulting from different sets of parameter, and thus operates as an orientation for the derivation of the set of parameters. Additionally, the study provides a framework for tuning the external drive with respect to various properties of the network related to STAS.

## Network architecture

In our study, we focus on EI-networks commonly seen throughout various brain regions. Each neuronal population is arranged on a square grid. The grid is folded to a torus to avoid boundary effects (Kumar, Rotter, and Aertsen 2008). The excitatory neurons populate a 70x70 grid ($npop_E$ = 4900), whereas the inhibitory population ($npop_I$ = 1225) is arranged on a 35x35 grid. In contrast to Spreizer et al. (2019), we placed the inhibitory neuron as center of four excitatory neurons to ensure that the distance of each excitatory neuron to the closest inhibitory neuron is similar, and vice versa (Figure 1-a).

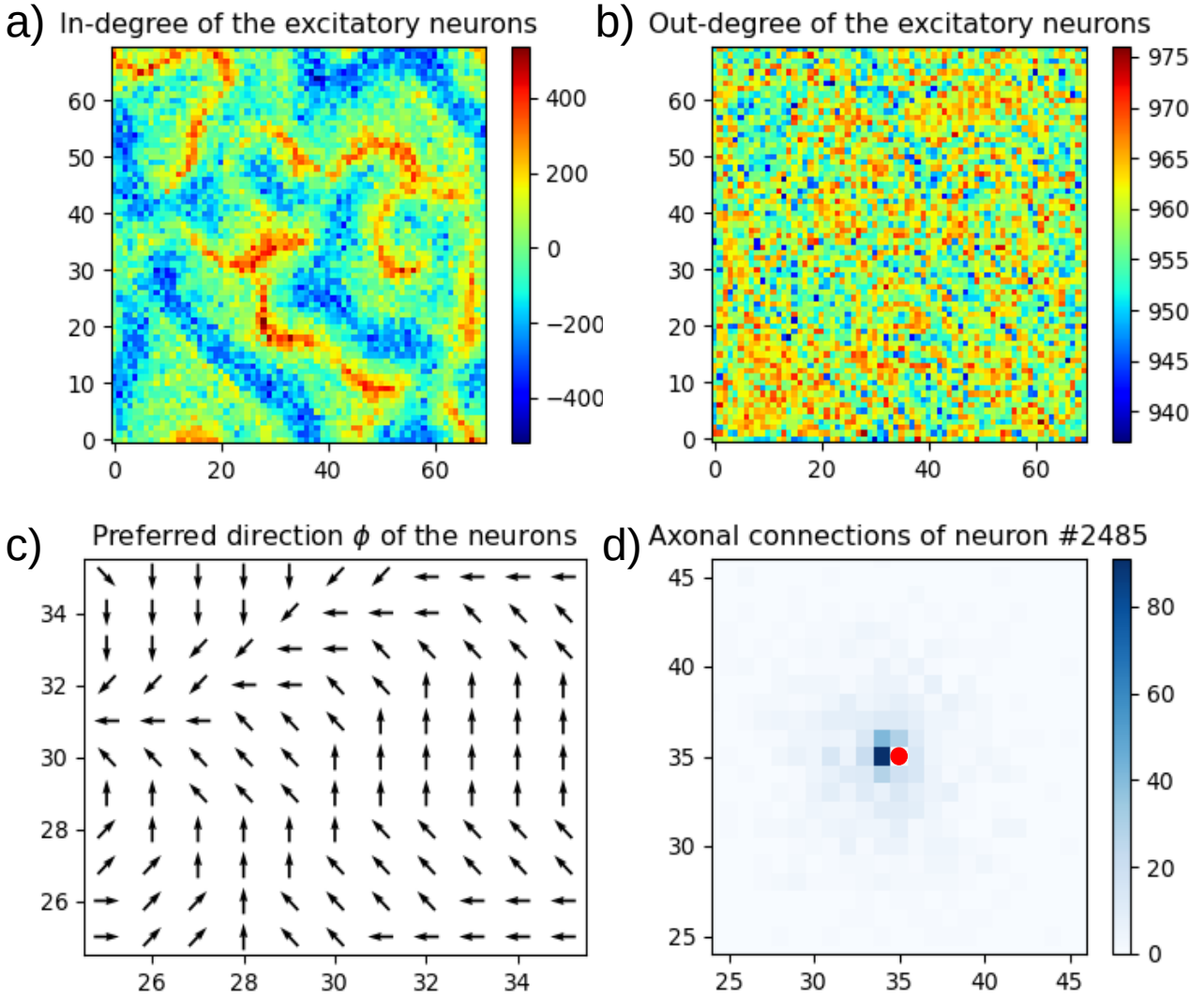


*Figure 2: Network configuration: a) Shows the in-degree of the excitatory population. Inhibitory synapses are multiplied with the ratio (*$\text{npop}_E$:$\text{npop}_I$ *= 4:1) and subtracted. b) the out-degree of the excitatory population is shown. c) The preferred direction ϕ is shown. According to the Perlin configuration, adjacent neurons show similar ϕs, whereas neurons far from each other are unrelated. d) The axonal directions of neuron #2485 (red dot) is shown.*

For the generation of the connectivity matrix, each neuron forms up to 980 and 245 synapses to the excitatory and inhibitory population respectively (20% connection probability on average). Multiple synapses to a target neuron are permitted, whereas self-connection was excluded.

Following Spreizer et al. (2019), a distance-dependent connectivity probability was employed to determine the axonal projections. The connection probability depended on the distance between neurons and is drawn from a Gaussian distribution. The standard deviation of the Gaussian distribution, also called the space constant, was $\sigma_E = 5$ for excitatory neurons, and $\sigma_I = 5$ for inhibitory neurons, with respect to the correspondent grid (scaled properly for projections to the other grid) (Figure 1-b). This connectivity method tended to have a high probability of connections within the vicinity, thus they form local recurrent random networks (LCRN) (Mehring et al. 2003).

In contrast to the configuration of Spreizer et al. (2019), we used a higher average connection probability, but since the population sizes were much smaller, the total number of connections per neuron was only slightly higher. This high number of connections resulted in a good representation of the Gaussian distribution. Thus the relative differences of synapses between adjacent target neurons was considered to be small.

Following the approach of Spreizer et al. (2019), we introduced the asymmetry of spatial connections from excitatory to excitatory neurons by the same algorithm. We made changes according to our different neuronal grid layout (Figure 2). The algorithm comprised the generation of Perlin noise (size: 4, base: 1), and assigned a preferred direction $\phi$ of the axonal projections to the neurons of the excitatory population (Figure 2-c). The synapses were shifted by one grid point in the direction of $\phi$. The Perlin noise and the shift were chosen such that we obtain a balance between the number of generated sequences and the tendency to change their direction. Additionally, the sequences travel with a moderate velocity (Spreizer et al., 2019). Note that the shift of synapses result in the formation of self-connections. Due to the constraints, these connections were removed. The resulting network is shown in Figure 2.

The in-, and out-degree are shown for the excitatory population only. For the in-degree, we calculated the sum of the incoming excitatory synapses and subtracted the inhibitory synapses, corrected for the ratio between the populations ($npop_E$:$npop_I$ = 4:1). The in-degree shows high variations between different locations arising from the fact that the preferred direction $\phi$ converged in some parts and diverged in others. In contrast, the out-degree takes only excitatory-to-excitatory synapses into account. Neither a high variation, nor regions with high-, or low-out-degrees are noted.

The internal drive was comprised of the activity of the neurons and the synaptic weights between them. In general, the synaptic weight was $J_X = 2$, and the inhibition factor was $g = 6.5$ resulting in excitatory weights of $J_E = J_X = 2$, and $J_I = -J_X \times g = -13$. To mimic ongoing activity as input to the network, each neuron received independent, homogeneous inputs from an external drive $I_{ext}$ (cf. eq. 1). This drive was modeled by a Gaussian white noise ($\mu = 25$, $\sigma = 20$). The balance of the internal and external drive was

critical, and hence we carefully set it with respect to the transfer function of the rate model ($x_0 = 50$, $s = 0.5$, cf. eq. 2)

*Effect of the neuromodulator*

For the simulations, we superimpose a circular patch of a neuromodulator, either DP or ACh, on the grid. The underlying neurons were affected, thus, as a consequence, the synaptic weight of incoming synapses is increased by 20% or decreased by 25%, respectively. These values were high enough to affect the STAS, but did not lead to overexcited, nor silent regions.

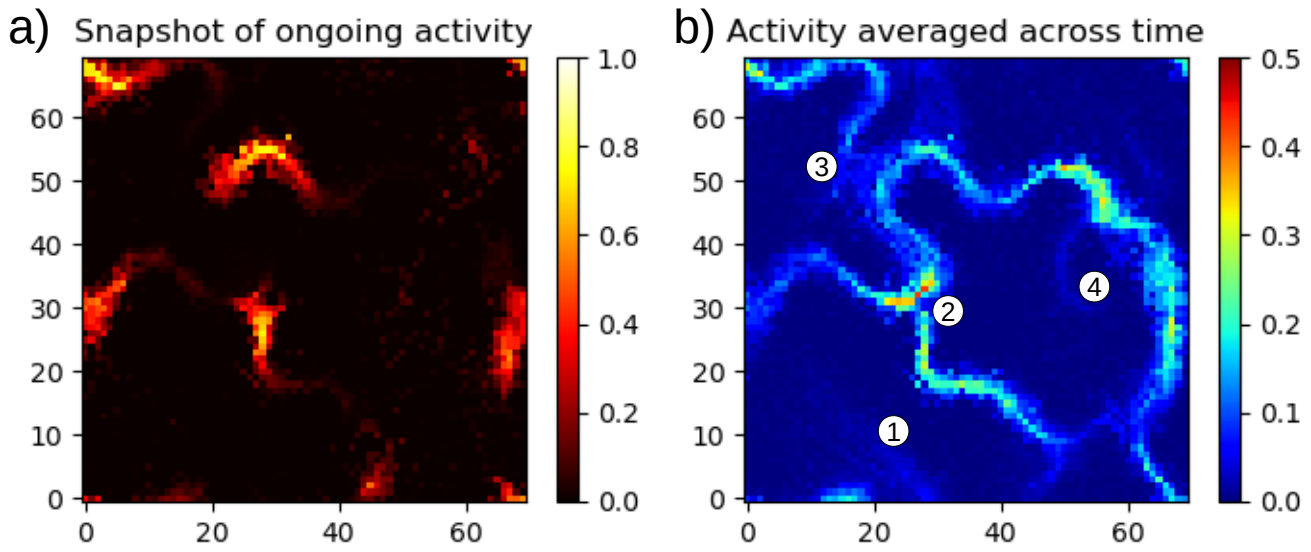


*Figure 3: Baseline simulation: a) a snapshot of the ongoing activity. b) The activity averaged across time. 1-4: Locations in which different characteristics are observable. Note the different scales of graph a) and b).*

## Simulation parameter

Each setup was simulated for $t_{sim} = 15{,}000$ ms with a simulation resolution of 1 ms. Given the randomness of the external drive, the outcome of a long simulation did not heavily depend on the initial conditions, but ensured that fundamental changes under test conditions became visible.

Before the data of the simulation was gathered, the network was given a warm-up time of $t_{warm} = 500$ ms. This warm-up allowed the network to get an active state, including STAS and silent regions. In simulations with patches, the warm-up was run without the effect of the neuromodulator. Consequently, the warm-up was not considered in any analysis.

## Analyses

The main focus of the analyses was on the excitatory population, because (1) the neuromodulator increases or decreases the excitability of this population, and (2) the STAS were easier to observe than in the inhibitory population.

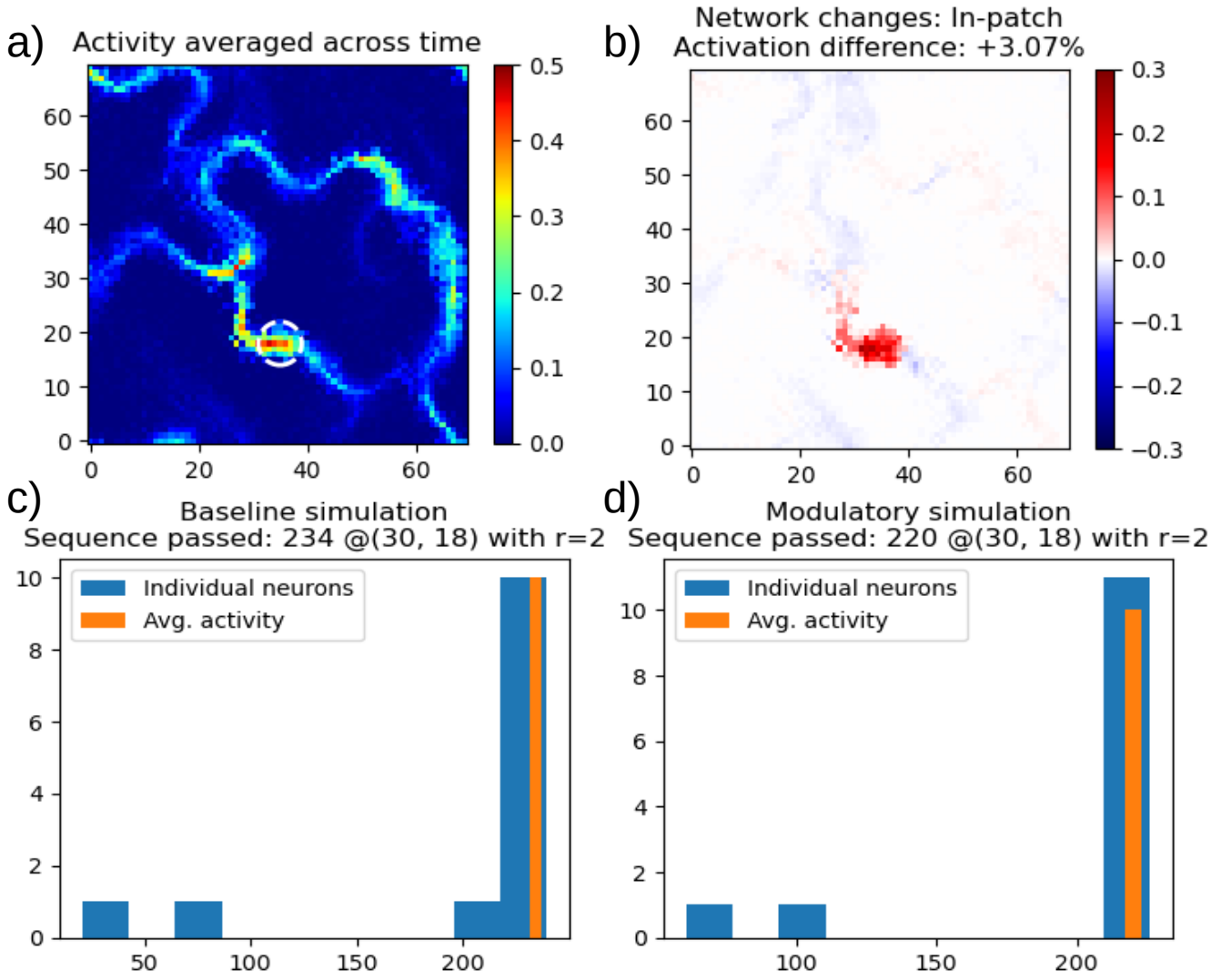


*Figure 4: In-patch: a) Average activity of modulatory simulation. Dashed circle display the DP patch. b) The difference of the average activation between the modulatory and the baseline simulation. c) and d) No. of passed sequences of the baseline and the modulatory simulation, respectively.*

*Average activity*

A simple analysis was to inspect the average activation of the neurons. Therefore, the activity of the neurons was averaged across all time points. High activation regions resulted from frequent activation

participating in sequences and/or strong activation. Occasional active regions and/or weakly active neurons only had a small amplitude due to the long simulation time.

*Effect of network changes on the average activity*

The change of the synaptic weights by introducing DP or ACh was expected to influence the average activation of the neurons. In order to visualize these differences, the average activity of the baseline simulation was deducted from the average activity of the modulated network. These differences had revealed the local effect in the vicinity of the neuromodulatory patch, as well as global effects.

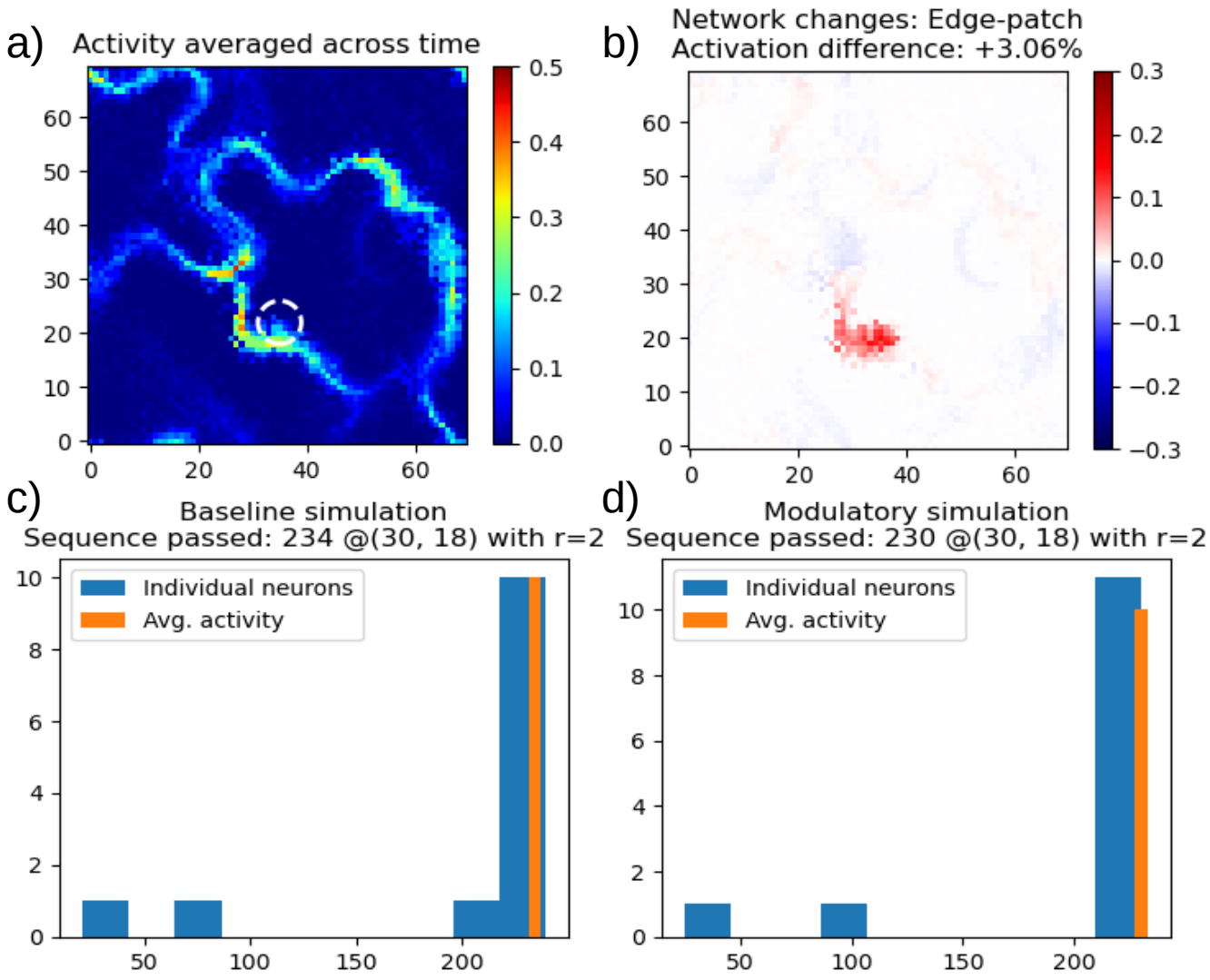


*Figure 5: Edge-patch: a)-d) see Figure 4.*

*Number of passing sequences*

Beside analyses on the average activity over time, we were interested in the number of passing sequences. Subsequently, we therefore identified the passing sequences by an algorithm comprised of two parts: in each part, the number of threshold (θ = 0.2) crossings was counted. The first part took a subset of neurons (usually we used 13 neurons that complied with the coverage of a circle with radius the r = 2), and detected the threshold crossing individually. The second part accounted for variability of the activation of the neuronal subset by averaging across neurons. Jointly, the detection gave a good estimate of the number of passing sequences, and also showed the variability of individual neurons. For visualization purposes, the height of the bar representing crossings of the average was increased.

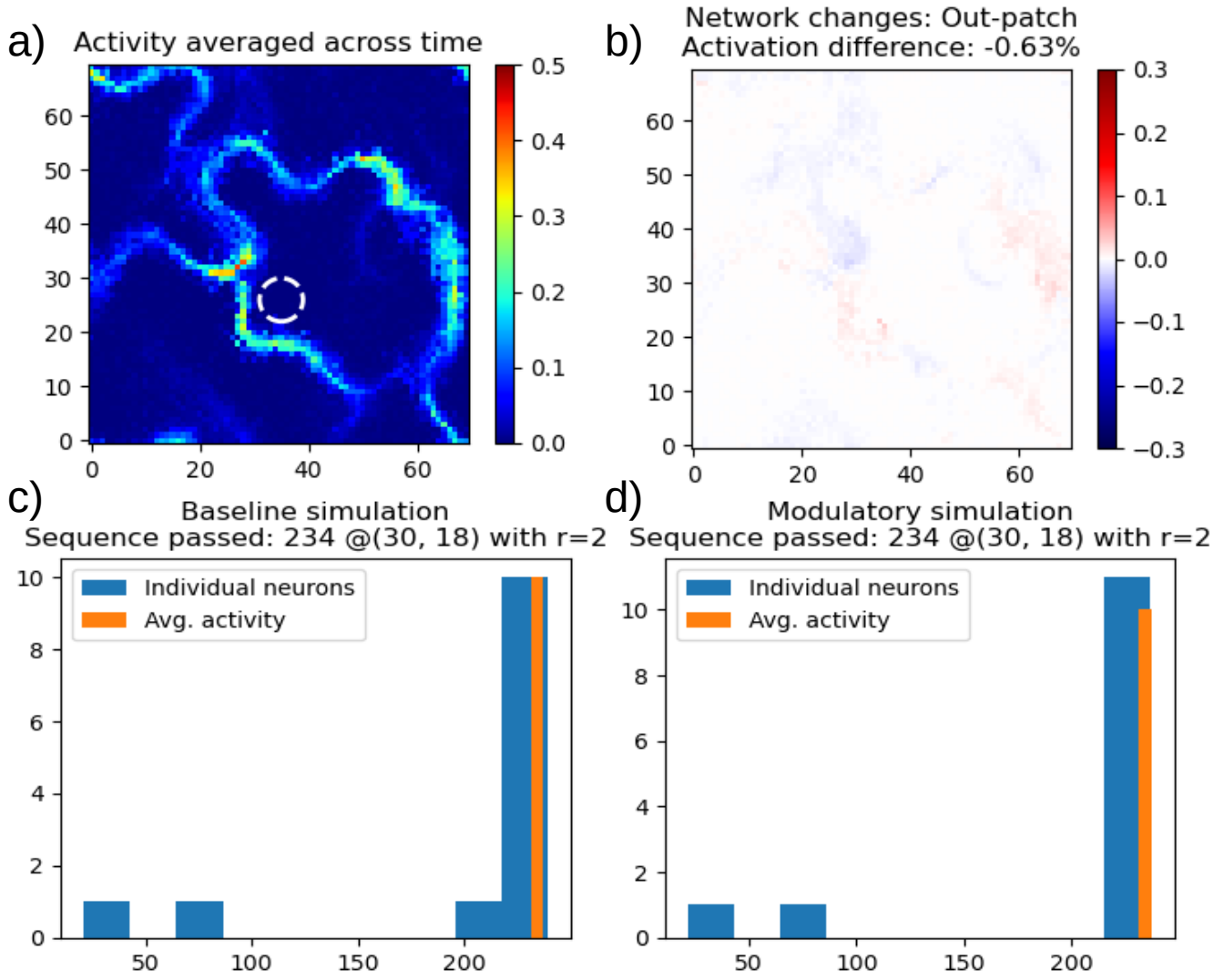


*Figure 6: Out-patch: a)-d) see Figure 4.*

*Neural manifold*

Sadtler et al. (2014) revealed a connection between neural manifolds and learning. Therefore, we wondered if DP could alter the neural manifold as a milestone in learning a new skill or behavior. To

account for this, we chose the simulation data of a modulated setup, and appended it to the baseline data for the neurons to be active in the same high-dimensional space. The next step was to employ a dimensional-reduction method, namely the principal component analysis (PCA) (Cunningham and Yu 2014). The PCA analyzes a data set described by inter-correlated variables and finds a new set of orthogonal variables, called principle components (PCs), along the axes of highest variance within the data set (Jolliffe and Cadima 2016). In order to inspect the manifolds, the complete data set was projected to the first three principle components. We focused on two versions: (1) local neural manifold, which accounts for the activity of a neural subset (circular shape with a radius of 8), and (2) the global manifold covering all remaining neurons.

## Results

In this section, we established multiple simulations by considering different locations of modulatory patches, that might influence the characteristics of STAS. Initially, we simulated the network without any modulation. We refer to this simulation as *baseline*. By inspecting the network, we expected strong activation in regions with a high in-degree (Figure 2-a). Moreover, sets of neurons sharing the same preferred direction could participate actively in STAS (not shown)**.**

In contrast to a network of spiking neurons, we inspected the activity of neurons on a continuous scale, but not by discrete spiking events. Thus, we examined the neural activity to derive characteristics of the STAS in the given network. In several locations in the network, clusters of increased activity occured, and moved across the network. We refer to these traveling clusters as STAS (Figure 3). Generally, the STAS showed strong activation in the center with decreasing activation towards the edges. Most of the sequences had a width of around six neurons, but were broader or narrower in other locations.

STAS started and terminated in various locations. One exception might be a specific path the STAS fared along. Since the neurons were arranged on a toroidal grid, this path were activated in a regular fashion. Once active, a sequence could travel along the path many times. We called this the *main path*. In contrast, STAS on other paths were active less often, and the STAS faded soon. We named these paths *branches* (e.g 1 in Figure 3-b). At some locations, we observed converging and diverging sequences, respectively (e.g 2 and 3).

Since this study focused on the impact of neuromodulators on the characteristics of STAS, we extrapolated locations, which might have the ability to change these characteristics. The first step, was to examine the effect of a modulatory patch on the STAS directly. So, we placed a patch inside, at the edge, and outside of a pathway. Secondly, a patch location was tested to increase the probability of the emergence of sequences. When the main path got active, we employed as patch location such that the STAS did not fade from time to time. Due to the converging and diverging character, we were interested in binary arithmetics. Specifically, we looked into patch locations to turn on or off pathways. Interestingly, we observed most STAS in regions of high in-degree, although there was one region that did not match this pattern. We investigated this region in a modulatory simulation (4 in Figure 3-b).

*In-, edge-, out-patch*

Initially, we investigated the effect of DP patches directly on or close to a path, but without diverging or converging branches in the vicinity. First, we placed a DP patch inside a sequence. We refer to this as in-patch simulation (Figure 4). The average activity did not show any qualitative changes of pathways STAS explore. However, the path on which the DP patch is active, increased the averaged activity at the patch, and subsequent to it. Decreased activity can be observed prior to the patch, which might result from stronger inhibition, due to a likewise more active inhibitory neurons in the patch. Moreover, the effect on the remaining network is divers. In total, the network is 3% more active compared to the baseline simulation.

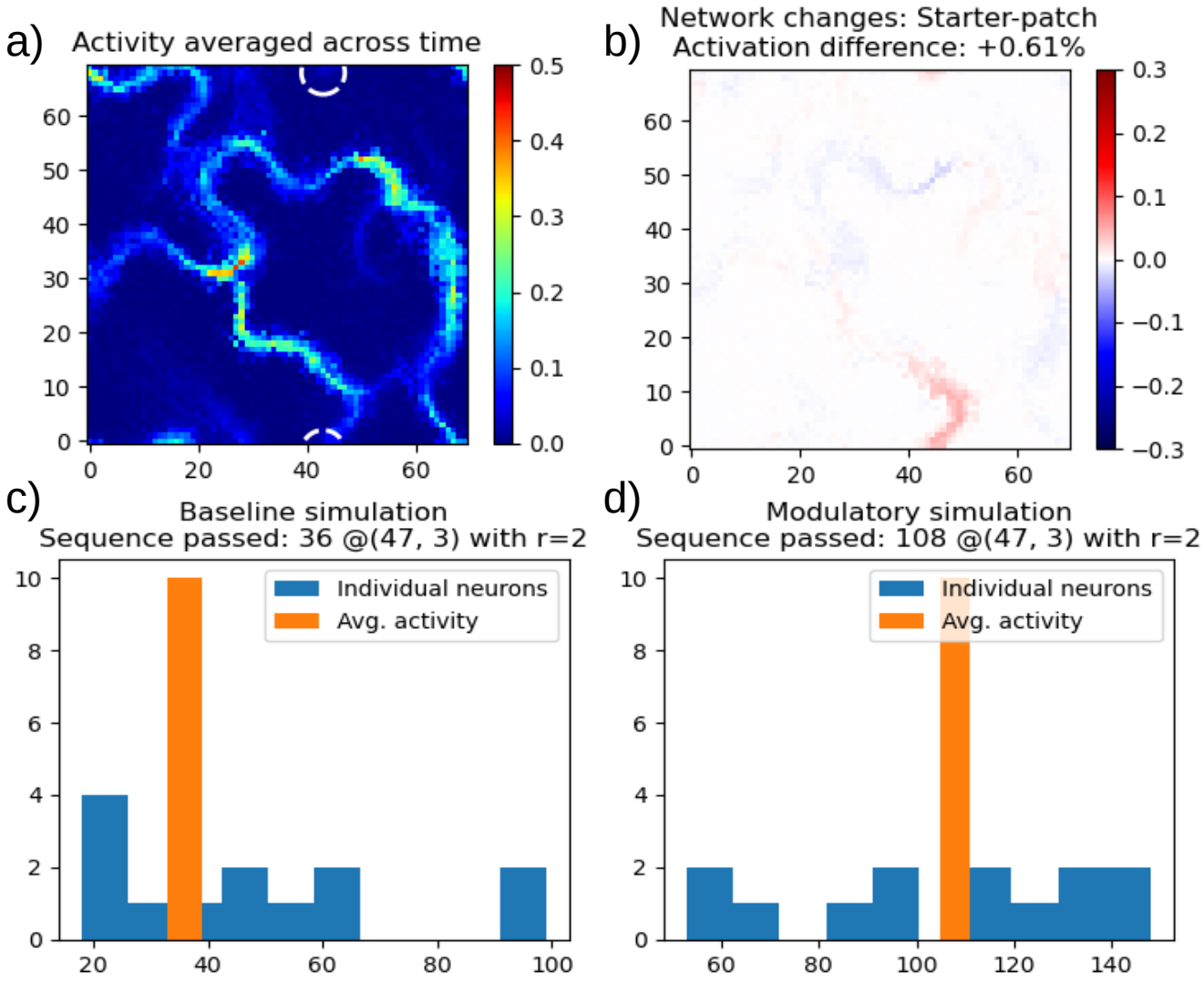


*Figure 7: Starter-patch: a)-d) see Figure 4.*

The number of STAS was measured closely behind the patch. In the baseline and the in-patch simulation, more than 200 STAS passed the patch. Although, the number decreased with the in-patch,

the overall number is still high. The small difference might be an indicator that the travel velocity of the STAS is affected by DP patches.

Secondly, the patch was moved orthogonally to the pathway to the edge of the path. We named it the edge-patch simulation (Figure 5). As for the in-patch, no new pathways were explored (Figure 5-a). Similarly, the same path was more active, but weaker than in the in-patch simulation. However, the increase of overall activity is virtually the same, despite the fact that the patch only covered the path partly. The reason was that other parts in the network were more active than in the in-patch simulation, but less active than in the baseline simulation (Figure 5-b, e.g. around (25, 40)). Moreover, the edge-simulation did not show inhibition prior to the patch. Interestingly, the number of passing sequences remained almost constant (Figure 5-c and -d).

Next, the patch was moved further orthogonally until it was outside of the path. We named it the out-patch simulation (Figure 6). As expected, there were neither qualitative changes in the pathways (Figure 6-a and -b), nor big changes in quantity. The average activity even decreased slightly, but the same number of sequences were detected (Figure 6-c and -d).
Overall, the in-patch showed strongest deviations from the baseline simulation. The edge-patch had less effect on the network changes, in average activation and passed sequences. The effects of the out-patch were mostly negligible. We concluded, that the patch size fitted the idea to influence the sequence to a certain degree, without creating patches of strong over-excitation. Moreover, we continued using patches inside of pathways.

*Starter-, repeater-, linker-patch*
Since, we investigated the effect of modulatory patches within one pathway, we were interested in other locations and therefore moving the patch along pathways. Most promising were regions, which evoked more complex activity patterns than merely transmitting a sequence. On these grounds, we selected regions in which STAS arise, fade, or diverge, respectively.

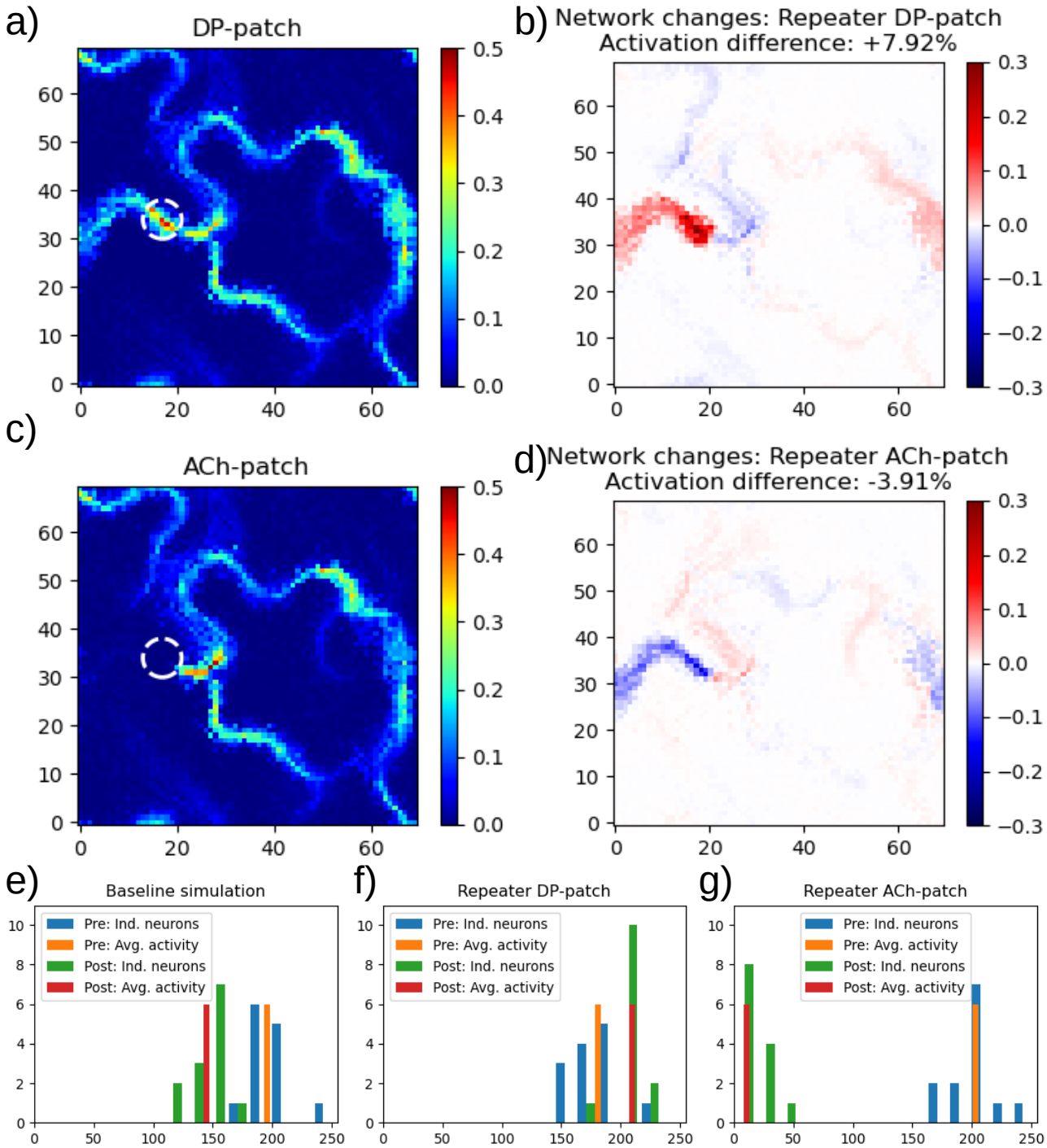


*Figure 8: Repeater-patch: a), c) Average activation across time with DP-patch or an ACh-patch respectively. b), d) Difference of averaged activity against baseline simulation. e)-g) No. of sequences passed for baseline, and repeater-patch (DP and ACh) respectively. Pre is measured at (29, 35) and detected 196 (baseline), 181 (DP-patch), and 203 (ACh) passed STAS. The post-location is at (2, 31) and measured 145, 210, and 11 sequences. The radius of pre and post was r = 2.*

All other modulatory simulations were dispensable when no STAS emerged in the network. Consequently, we situated a DP patch in the starting location of a sequence. We refer to as starter-patch (Figure 7). Commonly, the sequence is active now and then, and merges into the main path quickly. With increased excitability, the path was active more often, even tripled the number of passed sequences (Figure 7-c and -d). This also lead to stronger activation of the patch and the path on average over time (Figure 7-b). All in all, this starter-patch had a high impact on a local level on mainly one pathway. However, the change in the global activity might considered to be small.
Next, we observed that STAS on the main fade from time to time at around (17, 34). Unsurprisingly, that position had a low in-degree (Figure 2). Therefore, we aimed at increasing the stability of the main path, so that the sequences were able to pass this position. Since, we repeated the activation, we refer to this patch as repeater-patch (Figure 8). Initially, we set up a DP-patch to stabilize the main path. It turned out that the effect was more complex compared to the in-patch. In Figure 8-a and -b it is shown, that the repeater-patch raised the activation in the patch and subsequent to it, far into the main pathway. Also, it decreased the activity at around (25, 40), which was also part of the main, due to long-range inhibition. The total change of activity was more than twice as high as for the in-, or the edge-patch. The number of sequences also reflected these effects well. A strong boost from 145 to 210 detected STAS was observable behind the patch. In contrast, the amount went down from 196 to 181 sequences prior to the patch (Figure 8-e and -f).
As we controlled the main path in a more active fashion, we investigated the opposite setup by replacing the DP-patch by an ACh-patch. Remarkably, the ACh-patch showed the opposite effect in all analyses. Sequences on the main pathway faded most often, but sequences at around (25, 40) were more active. Consequently, the number of measured STAS pre patch went up slightly from 196 to 203. But post patch, the pathway was rarely active and only 11 STAS were detected. In total, the location of the repeater patch exhibited for higher excitability, as well as for depression strong and complex effects on the network activity.
At this point, we were able to start more STAS and increase the stability, specifically at weak points, where sequences tended to fade. To continue the exploration of locations that have a big impact on the emergence and/or the properties of STAS, we had a close look at regions with diverging pathways. Thus, we linked a branch to the main pathway in order to control the activity in that branch. To cover both trends, we placed the, so called, linker-patch in two variants - as DP- and as ACh-patch. The result of the simulation is shown in Figure 9.
The DP-patch increased the average activity by circa 3.78%, leading to a stronger activation of the branch (see upper left part in Figure 9-a and -b). On the contrary, this effect was inverted utilizing an ACh-patch (Figure 9-c and -d). These arguments were supported by the number of sequences passed. Post to the patch, we measured 148 STAS in the baseline condition, 196 for the DP-simulation, and only 27 behind the ACh-patch. Comparing these numbers with the pre-location of the analysis of the repeater-patch, one can see that the baseline successfully diverged 3 out of 4 times, whereas the DP-patch increased the diverging rate to virtually 100%. As in the repeater simulation, the ACh-patch was able to efficiently disconnect the branch.

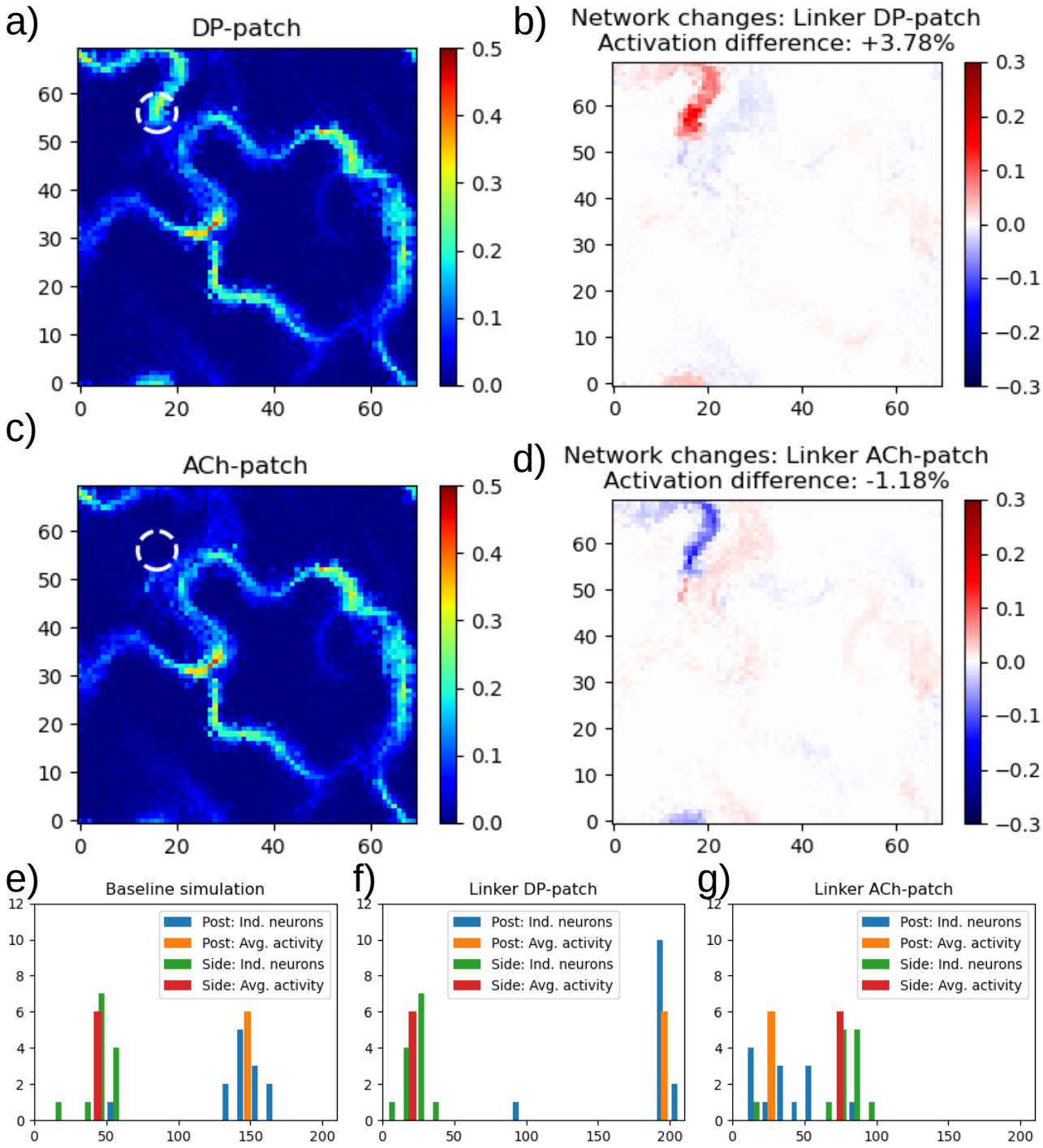


*Figure 9: Linker-patch: a), c) Average activation across time with DP-patch or an ACh-patch respectively. b), d) Difference of averaged activity against baseline simulation. e)-g) No. of sequences passed for baseline, and linker-patch (DP and ACh) respectively. Post is measured at (21, 65) and detected 148 (baseline), 196 (DP-patch), and 27 (ACh) passed STAS. The side-location is at (30, 61) and measured 44, 21, and 75 sequences. The radius of post and side was r = 2.*

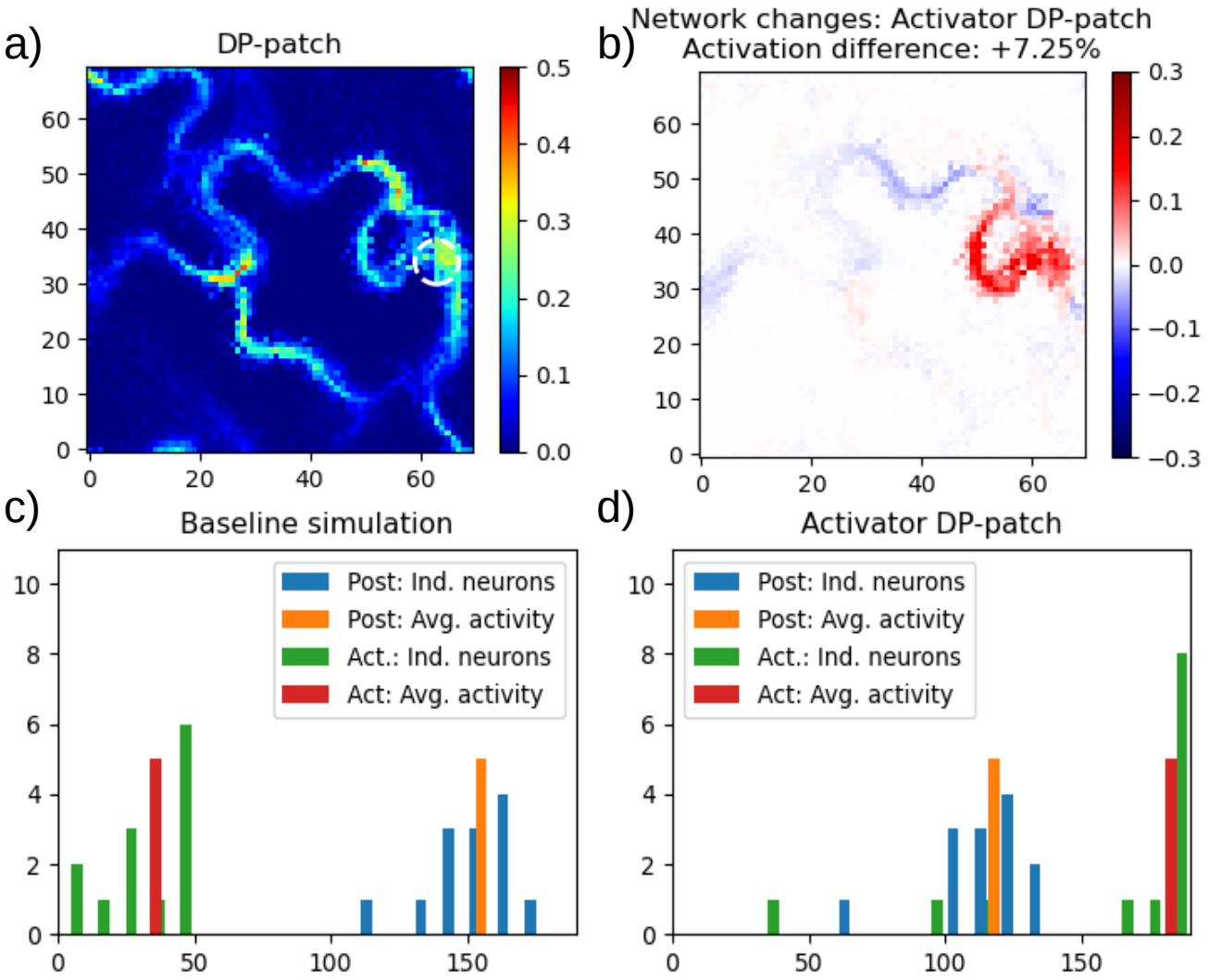


*Figure 10: Activator-patch: a), b) see Figure 4. c), d) No. of sequences passed for baseline, and DP activator-patch. Post is measured at (35, 49) and detected 155 (baseline), and 118 (DP-patch) passed STAS. The activator-location (act.) is at (49, 36) and measured 36, and 183 sequences. The radius of post and act. was r = 2.*

Although, the effects could be seen as local only, the patches influenced a neighboring pathway. This pathway was only active sometimes and can be barely seen in Figure 3-b. Since its higher activation, it became apparent in Figure 9-c around (30, 61). Hence, we ran the analyses also with regard to the side pathway. It turned out that, the elevated activity in the linked branch lead to a decline of sequences passed in the neighboring pathway, namely from 44 at baseline to 21. Vice versa, a suppressed branch incremented the sequence number to 75. In both ways, this was roughly a factor of two. We concluded two main points: (1) a patch can interact with multiple pathways even though the patch location itself infered only with one path, and (2) the post-locations of the repeater- and the linker-patch can be seen as bits indicating the appearance of specific patches. Straight forward, the bits might participate jointly

in a system based on our network that works as a binary logical operator (Boole, Grattan-Guinness, and Bornet 1999).

*Silent pathways*

Lastly, the inspection of the in-degree of the network (Figure 2-a) uncovered another phenomenon. Despite a high in-degree, one pathway (at around (50, 30)) was, surprisingly, mostly silent. We placed a DP-patch to activate the silent pathway. Similar to the edge-patch, we increased the excitability close to the active main, and connected it to the silent pathway (Figure 10). We called it the activator-patch. The silent pathway converges back to the main quickly.

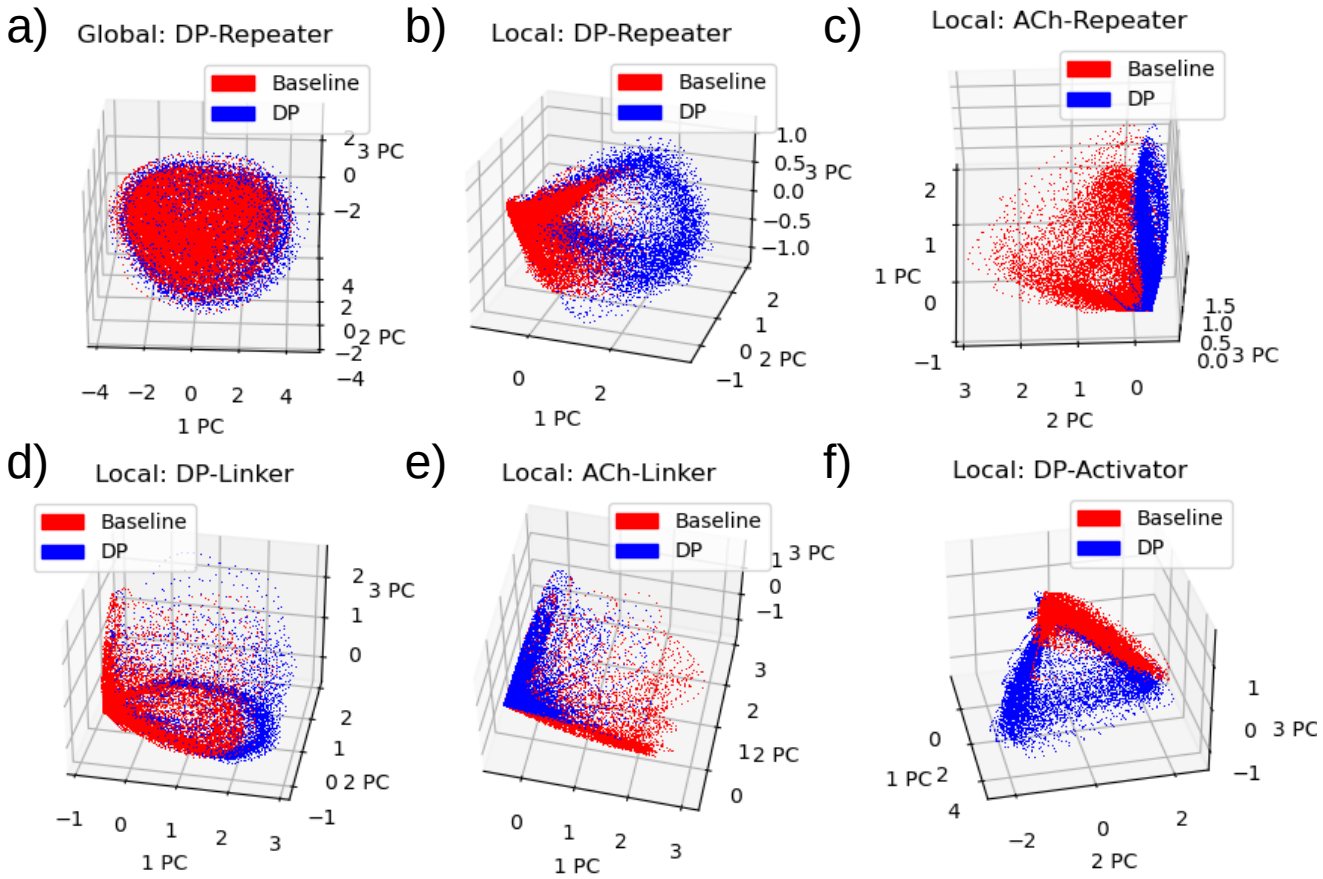


*Figure 11: Neural manifolds for global (a) and local (b-f) neural population.*

Interestingly, the silent pathway became very active, which is reflected by a strong increase of the average activation (Figure 10-a, and -b). Quantifying the activation of the silent pathway by the number of sequences passed, the rise is remarkable, namely from only 36 to 183. Moreover, the number of sequences going along the main decreased from 155 to 118 detected STAS. The reason might be found in the distance the STAS has to travel. By inspection, the silent pathway seemed to be longer than main path. Overall, a DP-in a specific region activateda silent pathway effectively.

In conclusion, we were able to control the pathways and sequences in several ways, therefore our interest switched to the investigation of the low-dimensional space the neuronal activity populate, and thus to the neural manifolds. The plots for the different patches exhibit mostly four different shapes: (1) spheric, e.g. Figure 11-a, (2) cylindric, e.g. -d, which might reflect a repeating activity, (3) conical, e.g. -b, which could stand for activity on multiple pathways, and (4) mostly flat, e.g. -c, representing low activity.

The effect on the global manifold was small, and none of the patches lead to a qualitative change (Figure 11-a). The repeater-simulation with a dopaminergic patch is shown as an example. Both traces are mostly overlapping – in all cases. The in-, edge-, out-, and starter-patch had a low impact on the local manifolds, and were comparable with the graph of a global manifold.

In contrast, DP- and ACh-patches had a more diverse effect on the neural manifolds locally (Figure 11-b to -f). The DP-repeater-patch displayed a conical shape. Most obviously, the extension of the traces is larger for the DP-patch simulation. This was caused by the increased activation of the pathway. Even though, the traces of both simulations covered mostly the same PC space, the baseline data was more present in one part of that space, whereas the DP data was in another part. Together, this mirrored the previous analyses.

The same simulation but with an ACh-patch showed very different results. As expected, the baseline simulation was conical again. However, the ACh data only populated a flat disc. This is in line with our previous results, due to the lack of activity in the pathway.

Interestingly, the linker simulation with DP-patch appeared in a similar fashion. Though, the basis was quite different. Here, we had two pathways – one branched from the main path often, and the neighboring path with occasional sequences. In this context, the traces in the PC space made sense. The baseline simulation exhibited STAS on both pathways, resulting in a conical shape. The DP activated the branch, and as a consequence inhibited the neighboring path. So, only the activity preferably lived in one part of the PC space.

The introduction of the ACh-patch also lead to a conical shape, but this time, the baseline and the ACh data seemed to live in different regions of the PC space. The traces are only slightly overlapping, and thus might stand for a change in the neural manifolds.

A more extreme version, can be seen in the trajectories of the activator simulation. On the one side, the baseline was active consistently. On the other side, the DP-patch introduced activation patterns that developed far more complex trajectories. Leading to the assumption that the neural manifolds might be very different from each other.

In conclusion, modulatory patches had diverse effects on the network activity. First, some patches influenced only one path (in-, edge-, out-patch), but do not alter the number of sequences in a large scale. Other patch locations altered the probability of STAS emergence (starter-), the stability (repeater-), or the effective connection of pathways (linker-patch). These effects might be bound to the vicinity of the patches, but might also interact with locations in distance (e.g. repeater). Due to long range inhibition, these local effects might infer with other pathways, although we employed only a single patch on one pathway in the simulations. Ultimately, the activator patch altered the activation

patterns to a high degree resulting in quite distinct trajectories of the PC space. In summary, patches of the same size had different interactions with the network. Hence, the patch location is crucial for the impact on the network. Moreover, the type of the neuromodulator was very important, because of the different signs of the DP- and the ACh-patches.

## Discussion

## Open Questions

1. Focus on the global changes of the patches.
    1. e.g. investigate how the starter patch affects the no. of passed sequences in the main path.

## References


1. Amari, Shun-Ichi. 1972. “Characteristics of Random Nets of Analog Neuron-Like Elements.” *IEEE Transactions on Systems, Man, and Cybernetics* SMC-2 (5): 643–57. https://doi.org/10.1109/TSMC.1972.4309193.
2. Bhalla, Upinder S. 2019. “Dendrites, Deep Learning, and Sequences in the Hippocampus.” *Hippocampus* 29 (3): 239–51. https://doi.org/10.1002/hipo.22806.
3. Boole, George, I. Grattan-Guinness, and G. Bornet. 1999. “George Boole: Selected Manuscripts on Logic and Its Philosophy.” *Studia Logica* 63 (1): 143–46.
4. Bouchard, Kristofer E., and Michael S. Brainard. 2016. “Auditory-Induced Neural Dynamics in Sensory-Motor Circuitry Predict Learned Temporal and Sequential Statistics of Birdsong.” *Proceedings of the National Academy of Sciences* 113 (34): 9641–46. https://doi.org/10.1073/pnas.1606725113.
5. Centonze, Diego, Gubellini, Paolo, Pisani, Antonio, Bernardi, Giorgio, and Calabresi, Paolo. 2003. “Dopamine, Acetylcholine and Nitric Oxide Systems Interact to Induce Corticostriatal Synaptic Plasticity.” *Reviews in the Neurosciences* 14 (3): 207–16. https://doi.org/10.1515/REVNEURO.2003.14.3.207.
6. Cunningham, John P., and Byron M. Yu. 2014. “Dimensionality Reduction for Large-Scale Neural Recordings.” *Nature Neuroscience* 17 (11): 1500–1509. https://doi.org/10.1038/nn.3776.
7. Day, Michelle, David Wokosin, Joshua L. Plotkin, Xinyoung Tian, and D. James Surmeier. 2008. “Differential Excitability and Modulation of Striatal Medium Spiny Neuron Dendrites.” *Journal of Neuroscience* 28 (45): 11603–14. https://doi.org/10.1523/JNEUROSCI.1840-08.2008.
8. Diesmann, Markus, Marc-Oliver Gewaltig, and Ad Aertsen. 1999. “Stable Propagation of Synchronous Spiking in Cortical Neural Networks.” *Nature* 402 (6761): 529–33. https://doi.org/10.1038/990101.

9. Gallego, Juan A., Matthew G. Perich, Lee E. Miller, and Sara A. Solla. 2017. “Neural Manifolds for the Control of Movement.” *Neuron* 94 (5): 978–84. https://doi.org/10.1016/j.neuron.2017.05.025.
10. Haga, Tatsuya, and Tomoki Fukai. 2018. “Recurrent Network Model for Learning Goal-Directed Sequences through Reverse Replay.” Edited by Upinder Singh Bhalla and Michael J Frank. *ELife* 7 (July): e34171. https://doi.org/10.7554/eLife.34171.
11. Hamid, Arif A., Michael J. Frank, and Christopher I. Moore. 2021. “Wave-like Dopamine Dynamics as a Mechanism for Spatiotemporal Credit Assignment.” *Cell*, April. https://doi.org/10.1016/j.cell.2021.03.046.
12. Jolliffe, Ian T., and Jorge Cadima. 2016. “Principal Component Analysis: A Review and Recent Developments.” *Philosophical Transactions of the Royal Society A: Mathematical, Physical and Engineering Sciences* 374 (2065): 20150202. https://doi.org/10.1098/rsta.2015.0202.
13. Kumar, A., S. Rotter, and A. Aertsen. 2008. “Conditions for Propagating Synchronous Spiking and Asynchronous Firing Rates in a Cortical Network Model.” *Journal of Neuroscience* 28 (20): 5268–80. https://doi.org/10.1523/JNEUROSCI.2542-07.2008.
14. Kumar, Arvind, Stefan Rotter, and Ad Aertsen. 2010. “Spiking Activity Propagation in Neuronal Networks: Reconciling Different Perspectives on Neural Coding.” *Nature Reviews Neuroscience* 11 (9): 615–27. https://doi.org/10.1038/nrn2886.
15. Lashley, K. S. 1951. “The Problem of Serial Order in Behavior.” *Cerebral Mechanisms in Behavior*, 112–146.
16. Mehring, Carsten, Ulrich Hehl, Masayoshi Kubo, Markus Diesmann, and Ad Aertsen. 2003. “Activity Dynamics and Propagation of Synchronous Spiking in Locally Connected Random Networks.” *Biological Cybernetics* 88(5): 395–408. https://doi.org/10.1007/s00422-002-0384-4.
17. Modi, Mehrab N, Ashesh K Dhawale, and Upinder S Bhalla. 2014. “CA1 Cell Activity Sequences Emerge after Reorganization of Network Correlation Structure during Associative Learning.” Edited by Howard Eichenbaum. *ELife* 3 (March): e01982. https://doi.org/10.7554/eLife.01982.
18. Pastalkova, Eva, Vladimir Itskov, Asohan Amarasingham, and György Buzsáki. 2008. “Internally Generated Cell Assembly Sequences in the Rat Hippocampus.” *Science* 321 (5894): 1322–27. https://doi.org/10.1126/science.1159775.
19. Patriarchi, Tommaso, Jounhong Ryan Cho, Katharina Merten, Mark W. Howe, Aaron Marley, Wei-Hong Xiong, Robert W. Folk, et al. 2018. “Ultrafast Neuronal Imaging of Dopamine Dynamics with Designed Genetically Encoded Sensors.” *Science* 360 (6396). https://doi.org/10.1126/science.aat4422.
20. Redgrave, Peter, Manuel Rodriguez, Yoland Smith, Maria C. Rodriguez-Oroz, Stephane Lehericy, Hagai Bergman, Yves Agid, Mahlon R. DeLong, and Jose A. Obeso. 2010. “Goal-Directed and Habitual Control in the Basal Ganglia: Implications for Parkinson’s Disease.” *Nature Reviews Neuroscience* 11 (11): 760–72. https://doi.org/10.1038/nrn2915.

21. Reynolds, John N. J., Brian I. Hyland, and Jeffery R. Wickens. 2001. “A Cellular Mechanism of Reward-Related Learning.” *Nature* 413 (6851): 67–70. https://doi.org/10.1038/35092560.
22. Sadtler, Patrick T., Kristin M. Quick, Matthew D. Golub, Steven M. Chase, Stephen I. Ryu, Elizabeth C. Tyler-Kabara, Byron M. Yu, and Aaron P. Batista. 2014. “Neural Constraints on Learning.” *Nature* 512 (7515): 423–26. https://doi.org/10.1038/nature13665.
23. Spreizer, Sebastian, Ad Aertsen, and Arvind Kumar. 2019. “From Space to Time: Spatial Inhomogeneities Lead to the Emergence of Spatiotemporal Sequences in Spiking Neuronal Networks.” *PLOS Computational Biology* 15 (10): e1007432. https://doi.org/10.1371/journal.pcbi.1007432.
24. Wilson, Hugh R., and Jack D. Cowan. 1972. “Excitatory and Inhibitory Interactions in Localized Populations of Model Neurons.” *Biophysical Journal* 12 (1): 1–24. https://doi.org/10.1016/S0006-3495(72)86068-5.
25. Wilson, H. R., and J. D. Cowan. 1973. “A Mathematical Theory of the Functional Dynamics of Cortical and Thalamic Nervous Tissue.” *Kybernetik* 13 (2): 55–80. https://doi.org/10.1007/BF00288786.
26. York, Lawrence Christopher, and Mark C. W. van Rossum. 2009. “Recurrent Networks with Short Term Synaptic Depression.” *Journal of Computational Neuroscience* 27 (3): 607. https://doi.org/10.1007/s10827-009-0172-4.
27. Zhou, Fu-Ming, Charles Wilson, and John A. Dani. 2003. “Muscarinic and Nicotinic Cholinergic Mechanisms in the Mesostriatal Dopamine Systems.” *The Neuroscientist* 9 (1): 23–36. https://doi.org/10.1177/1073858402239588.